AGU PUBLICATIONS

JGR

Journal of Geophysical Research: Space Physics

RESEARCH ARTICLE
10.1002/2015JA021269

Special Section:
Variability of the Sun and Its Terrestrial Impact VarSITI

# Thermal and dynamical perturbations in the winter polar mesosphere-lower thermosphere region associated with sudden stratospheric warmings under conditions of low solar activity

**Renata Lukianova[1,2], Alexander Kozlovsky[3], Sergey Shalimov[4,5], Thomas Ulich[3], and Mark Lester[6]**

[1]Geophysical Center RAS, Moscow, Russia, [2]Arctic and Antarctic Research Institute, Saint Petersburg, Russia, [3]Sodankyla Geophysical Observatory, Sodankyla, Finland, [4]Institute of Physics of the Earth RAS, Moscow, Russia, [5]Space Research Institute, Moscow, Russia, [6]Department of Physics and Astronomy, University of Leicester, Leicester, UK

**Abstract** The upper mesospheric neutral winds and temperatures have been derived from continuous meteor radar (MR) measurements over Sodankyla, Finland, in 2008–2014. Under conditions of low solar activity pronounced sudden mesospheric coolings linked to the major stratospheric warming (SSW) in 2009 and a medium SSW in 2010 are observed while there is no observed thermal signature of the major SSW in 2013 occurred during the solar maximum. Mesosphere-ionosphere anomalies observed simultaneously by the MR, the Aura satellite, and the rapid-run ionosonde during a period of major SSW include the following features. The mesospheric temperature minimum occurs 1 day ahead of the stratospheric maximum, and the mesospheric cooling is almost of the same value as the stratospheric warming (~50 K), the former decay faster than the latter. In the course of SSW, a strong mesospheric wind shear of ~70 m/s/km occurs. The wind turns clockwise (anticlockwise) from north-eastward (south-eastward) to south-westward (north-westward) above (below) 90 km. As the mesospheric temperature reaches its minimum, the gravity waves (GW) in the ionosphere with periods of 10–60 min decay abruptly while the GWs with longer periods are not affected. The effect is explained by selective filtering and/or increased turbulence near the mesopause.

**Key Points:**
- Mesospheric temperature and wind measured by the meteor radar and Aura MLS
- Signatures of SSW are observed if solar activity is low
- Ionospheric acoustic-gravity waves decay after the SSW onset

**Correspondence to:**
R. Lukianova,
r.lukianova@gcras.ru

**Citation:**
Lukianova, R., A. Kozlovsky, S. Shalimov, T. Ulich, and M. Lester (2015), Thermal and dynamical perturbations in the winter polar mesosphere-lower thermosphere region associated with sudden stratospheric warmings under conditions of low solar activity, *J. Geophys. Res. Space Physics*, *120*, 5226–5240, doi:10.1002/2015JA021269.

Received 27 MAR 2015
Accepted 31 MAY 2015
Accepted article online 3 JUN 2015
Published online 27 JUN 2015



## 1. Introduction

The Sodankyla Geophysical Observatory (SGO), geographic coordinates 67°22′N, 26°38′E, geomagnetic latitude 64.1°, is situated in the vicinity of the statistical southern edge of the stratospheric polar vortex. It is also close to the equatorial part of the nightside auroral oval in the ionosphere. The SGO contains several radio instruments for observations of the mesosphere, thermosphere, and ionosphere including a rapid-run ionosonde and all-sky interferometric meteor radar (SGO MR). The ionosonde and the SGO MR have been operating since April 2007 and December 2008, respectively. Recently, *Kozlovsky et al.* [2013] utilized the ionosonde data to reveal the statistical characteristics of the traveling ionospheric disturbances and ionospheric effects of the particular events such as missile destruction on 9 December 2009 [*Kozlovsky et al.*, 2014]. At the same time, a large collection of wind and temperature values measured by the SGO MR in the mesosphere-lower thermosphere (MLT) region at 80–100 km altitude has not yet drawn similar attention.

Several MRs have been deployed within the Arctic Circle. During the last years, their measurements have successfully been used to study the thermal and dynamic regimes in the high-latitude MLT region. The occurrence of wind oscillations reversals in the MLT in relation to planetary wave activity and circulation disturbances was demonstrated by *Hoffmann et al.* [2002] on the basis of radar wind observations at Andenes (69°N). *Meek et al.* [2013] analyzed the temperature distribution measured by the Eureka MR (80°N). The Eureka and Svalbard MR (78°N) wind data were compared to the model prediction [*Manson et al.*, 2011]. Recently, *de Wit et al.* [2014a] using the new generation of the MR located at Trondheim (63.4°N) investigated the gravity waves (GW) forcing in the high-latitude mesopause region and a particular behavior of GW during sudden stratospheric warming (SSW) [*de Wit et al.* 2014b]. During SSW filtering, conditions for upward propagating GWs are changed, resulting in a weakening of the westward GW forcing due to the disturbed stratospheric wind conditions.

The wintertime high-latitude middle atmosphere is of particular interest because it is characterized by strong variability and dramatic changes in temperature, dynamics, and composition. In the winter hemisphere, the

stratosphere is usually cold with a temperature of 200–210 K at ~25 km altitude because the air within the polar vortex has almost no radiative heating and it is isolated from the warmer midlatitude air. In such conditions, the eastward winter polar night jet dominates the stratospheric zonal mean flow. While the high-latitude stratosphere is cold due to reduced radiative input, the upper MLT is warm because of downwelling induced by the global meridional mesospheric circulation.

The winter polar stratosphere is often unstable and may experience dramatic changes associated with the occurrence of SSWs, when there is greatly increased temperatures within a few days occurring in midwinter. Such events are caused by enhanced planetary wave activity that induces a westward forcing and decelerates or even reverses the eastward polar jet.

Two defining criteria were specified by the World Meteorological Organization (WMO). For a major warming to occur, the following criteria need to be satisfied: (a) an increase in temperature, poleward from 60° latitude at 10 hPa of 40–60 K takes place in less than 1 week and (b) zonal mean zonal wind over the same region reverses. The minor warming, though similar to the major warming, is less dramatic. According to the definition of WMO, a stratospheric warming is called minor if (a) a significant temperature increase, i.e., at least 25 K in a period of week or less is observed at any stratospheric level, in any area of the winter time hemisphere and (b) the wind reversal from westerly to easterly is less extensive (i.e., the zonally averaged zonal wind does not reverse) and the polar vortex is not broken down [*World Meteorological Organization Commission for Atmospheric Sciences*, 1978].

The SSW perturbations are not confined to the polar stratosphere only but associated with specific vertical coupling processes influencing the MLT region [*Labitzke*, 1972; *Lysenko et al*., 1975; *Labitzke and Naujokat*, 2000]. It is now well recognized that a sudden cooling of mesospheric temperatures occurs during the SSW events. Stratospheric warming and simultaneous mesospheric cooling were predicted [*Matsuno*, 1971], modeled [*Liu and Roble*, 2002], and observed using different techniques such as satellites [*Siskind et al*., 2005], airglow [*Cho et al*., 2004], radars, and lidars [*Walterscheid et al*., 2000; *Hoffmann et al*., 2002; *Mukhtarov et al*., 2007]. Wind anomalies associated with the strength of the polar vortex extend to the MLT as well. Measurements in the mesosphere reveal wind reversals from the normal eastward to westward winds during SSWs. A transient westward polar jet allows upward propagation of smaller scale waves. In particular, the eastward propagating atmospheric GWs penetrate into the MLT while the westward propagating GWs are blocked in the stratosphere. The eastward propagating GW breaking may also contribute to the meridional circulation in the MLT region in such a way that a poleward-downward circulation is replaced by an equatorward and upward one [*Andrews et al*., 1987].

Obtaining high-resolution data from the MLT region is a challenge, and continuous ground observations of the mesospheric wind and temperature in the vicinity of the stratospheric polar vortex edge are still rare. Besides ground-based radars spaceborne instruments are used to remotely sense the atmospheric parameters. Powerful instruments capable of providing information on the horizontal and vertical structure of atmospheric layers are the Earth Observing System Microwave Limb Sounder (MLS) on board the Aura satellite. MLS measures temperature at high vertical resolution from the lower stratosphere to the lower thermosphere. The MLS observations have been used to compare and verify the MR temperature at high latitudes [*Dyrland et al*., 2010; *Meek et al*., 2013]. *Iida et al*. [2014] used the MLS data to study the January 2009 major SSW. In particular, it was shown that the reversal from westerly winds to easterly winds occurred earlier in the mesosphere in comparison with the stratopause level.

The SSW manifestations at the polar high altitudes $>$100 km are even less experimentally documented than those in the lower altitude. Recent research has focused on understanding the connections between SSW events in the polar region and the ionospheric responses at middle and low latitudes. Observations have demonstrated a thermal connection between SSWs and pronounced changes in the midlatitude ionosphere [*Goncharenko and Zhang*, 2008]. In the auroral latitudes, observations in the middle-upper atmosphere during SSW are limited and the measurements routinely performed in SGO provide an important new data set.

In this paper, we introduce the time series of temperature and neutral wind in the MLT region as measured by the SGO MR during the period of December 2008 to August 2014. These data are verified by the Aura MLT observations and supplemented by the rapid-run ionosonde observations of the GW amplitudes just

above the SGO MR location. The combination of these instruments is used to study the middle and upper atmosphere anomalies related to SSW. The second section of the paper briefly describes the instrumentation and data. In the third section we show the time series of the SGO MR data, and the fourth section is focused on the winter seasons when strong thermal and dynamic perturbations are observed. In section 5 the particular winter of 2008–2009 when a major SSW occurred is presented in more details including the temperature and wind variations. Signatures of GW activity at the ionospheric altitude inferred from the collocated ionosonde measurements are shown in section 6. We then discuss in section 7 the results of our observations and compare them with previous findings.

## 2. Instruments and Data

### 2.1. Ground-Based SGO Instruments

An all-sky interferometric MR was installed at SGO at the end of 2008. The radar transmits spherical VHF (36.9 MHz) waves and receives reflections from the trails of ionized gas left by meteors entering the atmosphere (meteor echoes). The radar employs one transmitter antenna. The receiving five-antenna array is arranged as an interferometer, and phase differences in the signals arriving at each of the antennas of the interferometer can be used to determine an unambiguous angle of arrival. The position of the meteor is then located in the sky with a range accuracy of 2 km and angular accuracy of about 2° in meteor location. The meteor trails occur at heights between 80 and 100 km. Several thousand meteors are detected each day, and the MR observations of the motion of their trails allow the determination of the neutral wind velocity at these heights. By measuring the position and radial velocity of meteor, the MR enables two orthogonal (zonal and meridian) components of the neutral wind to be obtained at ~3 km height intervals from 82 km to 98 km altitude as a function of time. Measurements and routine data analysis provide the determination of the direction/strength of wind at six height layers with 1 h time resolution. The daily temperature data at the height of maximum meteor detection at ~90 km are calculated from the decay time meteor trails based on the method described in *Hocking* [1999] and *Hocking et al*. [2001]. Although this method is successfully used for many years and provides suitable data of the mesospheric temperature, it is known the tendency for meteor radars to underestimate true values at low temperatures and overestimate at higher ones [*Hocking*, 1999]. To fix this problem, some linear correction with empirical coefficients is applied in the routine data processing; however, the coefficients may depend on local conditions, so that the temperature data may have a systematic offset. Nevertheless, the MR data are known to show well variations of mesospheric temperature [e.g., *Kim et al*., 2012]. Because of this we focus on the shape of temperature variations, and the absolute values are only briefly discussed in section 5.1.

Since April 2007, at SGO, a frequency-modulated continuous-wave chirp ionosonde operates performing one sounding per minute. The 1 min temporal resolution at high latitudes is unique, and the resolution makes it possible to reveal rapid changes in the ionosphere associated with traveling ionospheric disturbances (TIDs) at the heights of 150–210 km. At SGO, the TIDs were observed as quasiperiodic oscillations of the *F* layer virtual height detected at sounding frequencies 2.5–3.5 MHz. Height variations associated with TIDs in different frequency bands from 5–10 min to 60–120 min were determined using the technique developed in *Kozlovsky et al*. [2013]. It was shown that the amplitude of TIDs may reach 7 km and exhibit the seasonal and the solar cycle variations. In most cases, TIDs are manifestations of atmospheric GWs. Using the ionosonde data, we may estimate the characteristics of TIDs caused by GW that penetrate to the ionospheric height during the lower atmosphere perturbations, in particular those associated with SSWs.

### 2.2. Aura MLS

The Aura satellite was launched in 2004 into a Sun-synchronous, near polar orbit 700 km above the Earth. The Aura global coverage is from 80°N to 82°S, with ~13 orbits per day, passing through two local times at a given latitude. Four instruments on board the satellite measure trace gases in the atmosphere by detecting their spectral signatures. The Earth Observing System Microwave Limb Sounder (MLS) observes the faint microwave emissions from rotating and vibrating molecules from the Earth limb viewing forward along the flight direction, scanning its view from the near ground up to $>$90 km. Temperature and geopotential height (GPH) at 54 levels from 1000 to 0.0001 hPa along each orbital track are available from the MLS [*Waters et al*., 2006]. The MLS vertical resolution is approximately 4 km in the stratosphere and 8 km from

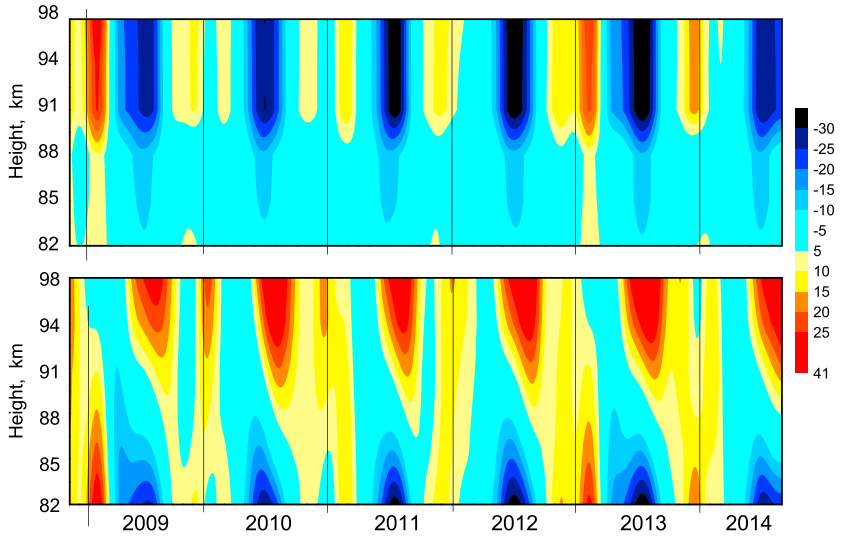


**Figure 1.** Height time series of the (top) meridional and (bottom) zonal winds in m/s covering altitudes 82–98 km over SGO from December 2008 to August 2014. Northward and eastward wind is positive (red); southward and westward wind is negative (blue). The shading interval for the wind speed is 5 m/s.

stratopause to mesosphere. The precisions of temperature and GPH vary from 1 K and 40 m in the upper stratosphere to 2.5 K and 100 m in the mesosphere. The horizontal resolution for temperature is ~170 km along the orbital track and 12 km cross track.

The MLS height data L2 V003 (version 3.3, Level 2) are used to construct the time series of daily temperature values over Sodankyla. The data quality is described in *Livesey et al.* [2013]. Data from latitude 67.5°N and longitudes within 16.4–36.4°E (10° to the east and to the west from the SGO longitude) are included in the analysis. Temperatures from the two longitudinally spaced tracks are linearly interpolated and centered to 26.4°E. The geographical bin 67.5°N, 26.4 ± 10°E is usually crossed twice a day, at about 12 and 17 UTC. To obtain the daily vertical temperature profiles, the values from the ascending and descending nodes are averaged. The MLS observations cover the whole time interval of the SGO MR observations and available on a daily basis with very few gaps.

## 3. SGO MR Observations

The SGO MR measurements form the main experimental basis for our analysis of the wintertime mesospheric wind and temperature anomalies. The SGO MR database of the 1 h values of meridional and zonal components of neutral wind now contains almost 6 years of observations. The zonal and meridional winds at the altitude range between 82 and 98 km, as measured by the SGO MR from 1 December 2008 to 31 August 2014, are shown in Figure 1. In the figure, the hourly values are averaged over a day and then smoothed by a 31-point fast Fourier transform filter, and the color coding shows the wind direction and magnitude.

The annual pattern dominates of the wind vector. Also, both the zonal (Figure 1, bottom) and the meridional (Figure 1, top) winds exhibit a prominent year-to-year variability. The common feature of the altitudinal distribution is that the wind regime is completely changed at ~90 km height. Above 90 km, the meridional wind is strong and seasonally dependent. The summer meridional wind is southward (negative), and its speed may reach 40 m/s. The winter meridional wind is less stable and mostly northward (positive) with the speed varying from 5 to 30 m/s. The strongest northward winds occur in the beginning of 2009 and 2013. In some midwinters (e.g., in 2010–2011) the southward turning is observed. Below 90 km, the meridional wind shows little variation being mostly southward all over the year with the speed reduced to 5–10 m/s.

The zonal wind seasonal pattern is more complicated. The gradual descending of the summertime eastward (positive, westerly) wind and the existence of the shear layers of zero wind is clearly seen in Figure 1 (bottom).

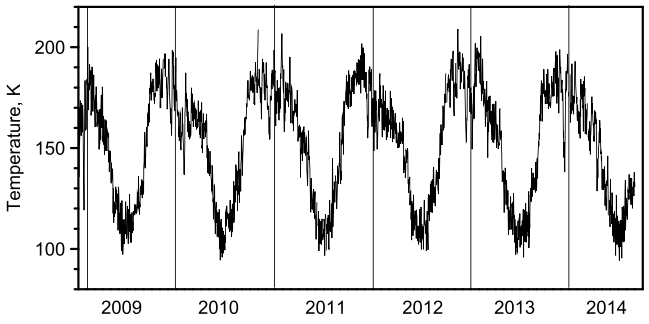


**Figure 2.** Temperature at ~90 km height over SGO from December 2008 to August 2014.

In summer, the higher altitude (>90 km) eastward wind speed reaches 30 m/s, while the westward wind of ~30 m/s flows below 90 km. In winter, the zonal wind is mostly eastward at the entire altitudinal range. The winter zonal wind pattern is rather unstable and varies considerably in speed and direction from month to month and from year to year. For example, in the late winters of 2009 and 2013, the lower altitude zonal wind turns more to the east in comparison with the other years. Note that since the plots in Figure 1 are based on the monthly averages, the daily values of the wind velocity may differ considerably from this representation.

On the basis of the height profile of the meteor decay time, the temperature is calculated using the technique described by *Hocking* [1999]. Figure 2 shows the daily values of temperature at ~90 km altitude (the approximate altitude at which the majority of meteor trials are detected by MR). The annual pattern dominating in the temperature record consists of warm winters and cold summers. The temperature increases rapidly from the summer minimum of ~120 K to the winter maximum of ~180 K, thereafter decreasing until the next summer. The daily values are more perturbed in winter within about 20 K, and the daily temperature may suddenly drop down to 150 K or even below. The strongest midwinter sudden cooling occurred on January 2009 while the weaker coolings are seen in some other years. These temperature anomalies are associated with major and minor SSWs which occurred in the winter polar stratosphere. Also, regular negative excursions are seen in mid-December. These anomalies are not related to SSWs but due to the specific sort of meteors occurred each year at the Earth's orbit. This phenomenon will be considered in a subsequent paper.

## 4. Wintertime Thermal and Dynamic Anomalies in 2008–2014

### 4.1. Zonal Mean Temperature and Wind in the Stratosphere

The main characteristics of SSWs are a rapid warming by tens of degrees in just a few days with a reversal in the normal latitude temperature gradient and a dramatic decrease or reversal in the zonal mean eastward winds in the winter vortex. Figure 3 shows the daily means of temperature and the daily values of mean zonal wind at 60°N at the pressure level of 10 hPa which is a representative altitude (~25 km) for the detection of the SSW events. The superimposed plots for the 4 month period from December to March of each year from 2009 to 2014 are shown. The data were obtained from the NASA Goddard Space Flight Center Annual Meteorological Statistics of Modern Era Retrospective Analysis for Research and Applications (MERRA) [*Rienecker et al*., 2011].

Figure 3a depicts the evolution of stratospheric temperature for the winters 2008/2009–2013/2014. Several temperature enhancements that usually peaked in January occurred in the northern stratosphere. The largest midwinter warming of 250 K occurred on 23 January 2009. During four winters (defined according to its January) in 2010, 2012, 2013, and 2014, the temperature increased from ~200 K up to ~230 K, and in 2011 the warming began earlier and hardly reached 230 K. Figure 3b depicts the evolution of the stratospheric zonal wind at 10 hPa. In the winter stratosphere, the eastward directed flow usually dominates and circulation undergoes significant changes during the occurrence of a SSW. Strong reversals of westerly polar jets occurred on 24 January 2009 and 5–6 January 2013. In 2010, the westerly jet was considerably decelerated and slightly reversed 2 times in mid-February. In 2011, a deceleration of westerlies from ~35 to ~15 m/s occurred, while in 2012 and 2014, the polar vortex was slightly disturbed. Thus, two from six events (on January 2009 and 2013) may be classified as major SSWs according to WMO definition (though in 2013, the increase in temperature is a bit less than 40 K). The 2009 major SSW is among the most intense events in the Northern Hemisphere since the beginning of observations [*Labitzke and Kunze*, 2009]. The events of 2012 and 2014 are minor warmings because of no reversal in zonal wind,

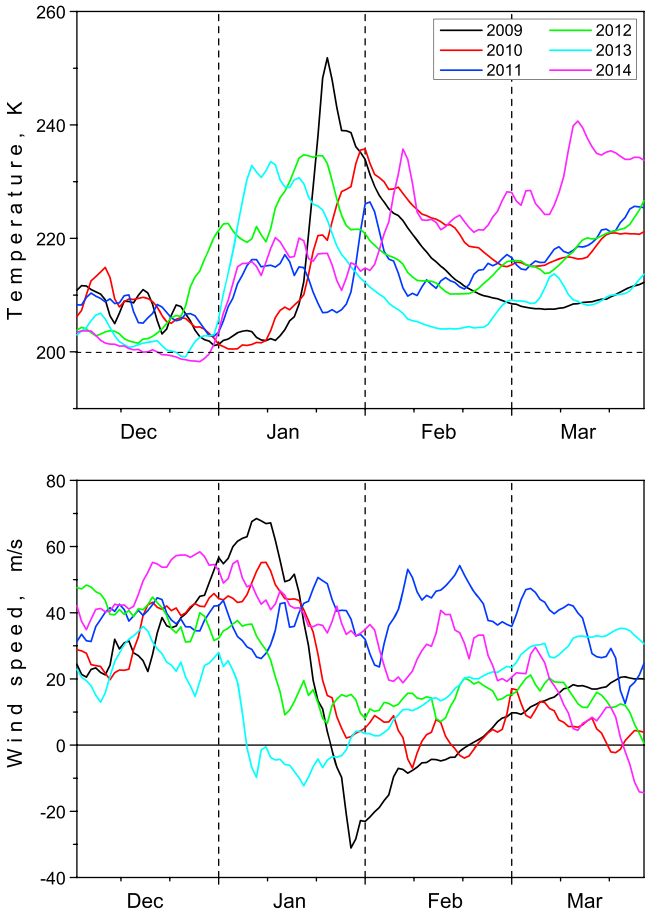


**Figure 3.** (a) Stratospheric temperature poleward from 60°N and (b) the zonal mean zonal wind at 60°N at the pressure level of 10 hPa. The 4 month intervals from December of the previous year to March of the current year for winters from 2008 to 2014 are superimposed.

while the event of 2010 can be considered as a medium warming. Though the WMO does not provide a strict definition for medium warmings, the event of 2010 can be considered as a very weak major SSW and here we call it a medium one.

### 4.2. Mesospheric Temperature From SGO MR

The stratospheric anomalies are related to the mesospheric disturbances as measured by the SGO MR. Figure 4 depicts the daily values of MR temperature from 1 January to 15 February for each year from 2009 to 2014. The temperature plots for six winters are superimposed in the same manner as in Figure 3 but a for shorter interval of time. December and March are excluded because during these months the stratospheric perturbations are relatively small. Because SSWs are picked in January, the MR temperatures are shown for the 1.5 months period only. Figure 4 shows that during all winters the SGO MR observes fluctuations of the MLT temperature in the range of 150–200 K. Two coolings with a temperature drop below 150 K stand out from the others. The largest drop, when the magnitude of cooling was around 50 K relative to the seasonal trend, occurred during the major SSW of 2009. The minimum of 120 K in MLT temperature occurred on 22 January while the stratospheric maximum of 255 K was detected on 23 January, i.e., a day later. In 2010, during a medium SSW, the magnitude of mesospheric cooling was around 30 K and minimum of 135–137 K occurred on 28–29 January. The corresponding stratospheric maximum of 235 K was reached on 30 January. During the other four winters, the temperature variation was irregular with no pronounced minimum. In particular, no mesospheric cooling was observed during the major SSW of 2013.

A possible reason for the different mesospheric temperature response to a SSW includes the level of solar activity during which a SSW occurred. In 2009 and 2010, the solar and geomagnetic activities were at a deep minimum [*Russell et al.*, 2010]. In 2009, almost no sunspots were observed in the Sun. In particular, according to the OMNI 2 database, the sunspot number (SSN) averaged over January–February 2009 was equal to 1.3. The solar radio flux at 10.7 cm wavelength ($F_{10.7}$ index) was less than 70. In 2010 the Sun became more active, but the SSN was still low: SSN = 15 and $F_{10.7}$ = 80 in January–February. Due to that reason, solar and geomagnetic modulation of the Earth's atmospheric circulation was reduced and mostly the intra-atmospheric dynamical processes were visible. In 2011–2014, the ascending phase of the 11 year solar cycle, the solar activity considerably increased. The major SSW of 2013 occurred at the maximum of solar cycle 24, when the SSN and $F_{10.7}$ averaged over January–February are 51 and 113, respectively. In 2010, the medium SSW was also accompanied by prominent mesospheric cooling. The SSW in 2010 is considerably less intense than that occurred in 2009 but with very similar characteristics in the MLT region. Under high solar activity conditions, the SSW signature is seen in the stratosphere but not in the

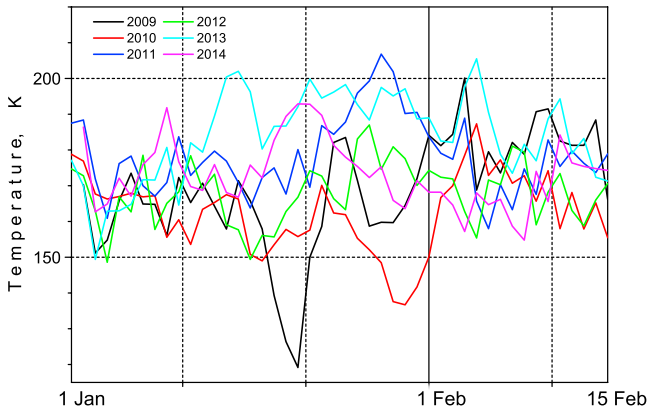


**Figure 4.** Mesospheric temperature at ~90 km height from the SGO MR. The 1.5 months intervals (1 January to 15 February) for 2008–2014 are superimposed.

mesosphere. It is likely related to the fact that the MLT region over Sodankyla attains additional energy from above: due to Joule heating of the auroral ionosphere because of stronger electrojets and particle precipitation and, to some degree, the direct absorption of solar UV radiation. In such conditions, the SSW-related cooling in the MLT region is poorly observed.

Due to the extremely low solar activity in 2009, a sudden mesospheric cooling associated with major SSW provided a unique opportunity to study the stratosphere-mesosphere-ionosphere coupling. In the next sections, we focus on the major SSW of 2009 (SSW2009) by looking in more detail at the temperature and wind perturbations in the MLT region over Sodankyla as measured by the space- and ground-based measurements. Then the results of the ionospheric sounding performed simultaneously by the SGO rapid-run ionosonde are presented.

## 5. Mesospheric Parameters Measured Over Sodankyla During SSW2009

### 5.1. Temperatures From SGO MR and Aura MLS

The meteor trail echo decay rates detecting by the ground-based SGO MR provides daily temperatures in the MLT near 90 km. The same region is observed by MLS from space. Figure 5 shows together the daily values of temperature measured locally by these two different instruments. The MR temperatures are shown as filled circles, while the MLS temperatures at the same height are shown as empty circles. Also, the stratospheric (10 hPa GPH) temperatures measured by MLS (asterisks) over Sodankyla and the daily means of temperature from MERRA (black line) are shown for the 1.5 month period from 1 January to 15 February 2009.

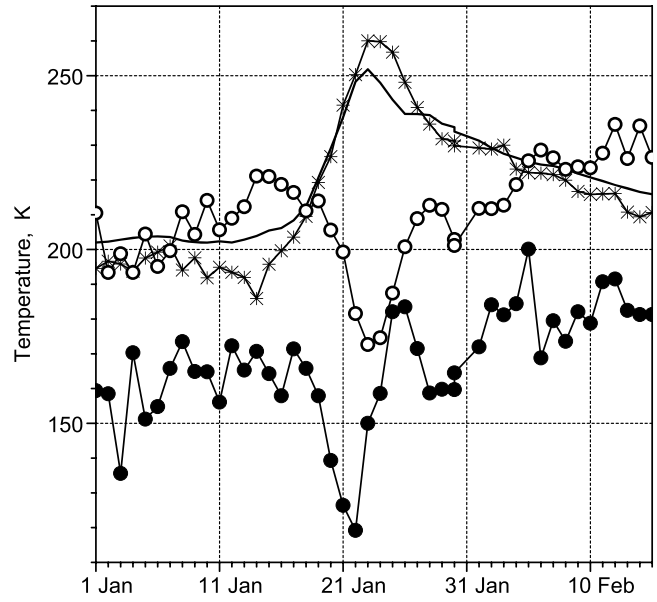


**Figure 5.** Daily averaged mesospheric temperatures at ~90 km from the SGO MR (filled circles) and MLS (empty circles); stratospheric temperatures at ~25 km from MLS (asterisks) and MERRA (black line) from 1 January to 15 February 2009.

The undisturbed stratospheric temperature at 10 hPa GPH is approximately 200 K. The SSW signatures are clearly seen as an abrupt increase of the stratospheric temperature and simultaneous decrease of the mesospheric temperature. According to both the MLS instrument locally and the MERRA reanalysis over 60°N, the stratosphere starts to warm just after 15 January. On 23 January, the temperature reaches its maximum of 260 K (MLS) and 250 K (MERRA) and gradually decreases afterward. According to the SGO MR, before 17 January the undisturbed mesospheric temperature is about 180 K. The mesospheric cooling is developed simultaneously with the stratospheric warming. Consequently, the temperature variations measured by MLS and SGO MR show negative bays. On 22 January, it drops down to 120 K forming

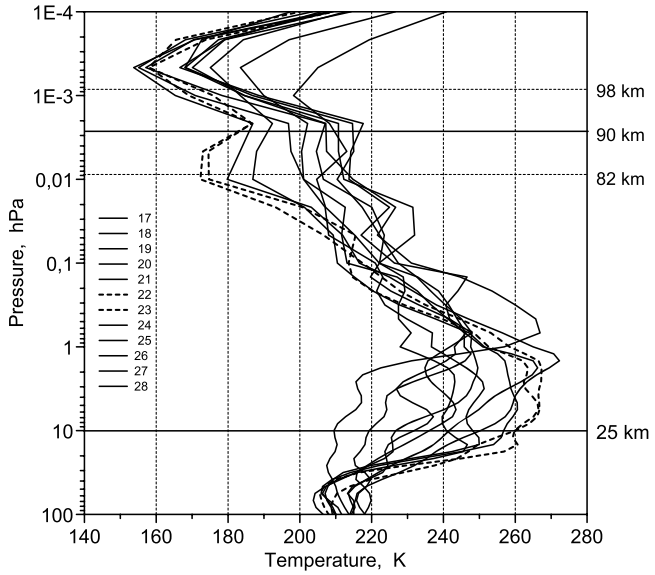


**Figure 6.** Vertical temperature profiles as observed with the MLS at the altitudinal range from 100 to 0.0001 hPa over SGO on 17–28 January 2009. The profiles corresponding to the peaks of the stratospheric warming and mesospheric cooling (22–23 January) are marked by dash lines.

a deep minimum. The MLS temperature variation agrees in shape and magnitude with that observed by SGO MR, but the radar gives significantly lower temperatures (a 25–30 K offset) than MLS. Most probably, the offset indicates a systematic error in the MR temperature estimate, which is the known feature of radars mentioned in section 2.1. However, for confirming reliability of the present result, it is important that both instruments, SGO MR and MLS, show the mesosphere cooling over Sodankyla by the same value of the order of 50–40 K. The amplitude of the corresponding stratospheric warming is ~60 K. It is also notable that the SGO MR minimum (22 January) occurs 1–2 day ahead of the stratospheric maximum (23–24 January). There is also a secondary cooling pulse on 27–30 January that is possibly related to wave activity.

### 5.2. Vertical Temperature Profiles From the Aura MLS

The values of the MLS temperatures presented in Figure 5 are inferred from the vertical temperature profiles available from the original Aura data set via the Mirador tool. The profiles are from the altitude range from 1000 to 0.00001 hPa GPH in which levels above 0.001 hPa are not reliable [*Livesey et al.*, 2013]. For comparison with the SGO MR observations, the MLS temperatures from the pressure levels of 0.0046 and 0.001 hPa (that roughly comprises the height of the meteor echoes) are used. As mentioned in section 5.1, there are usually two satellite passes per day within ~10° longitudinal intervals over Sodankyla. To obtain the daily vertical temperature profiles, the values from the ascending and descending nodes are averaged.

It is of interest to see, how the MLS vertical temperature profiles evolve before, during, and after the SSW. In particular, vertically narrow thermal inversion layer of ~10 K that is superimposed upon the normally decreasing temperatures of the upper mesosphere and occurred predominantly between 90 and 100 km in altitude [*Meriwether and Gerrard*, 2004] may affect the MLS temperatures selected for the comparison with the SGO MR temperatures.

Figure 6 displays each of the 12 days ranging from 17 January to 28 January 2009 vertical temperature profiles at the altitudes from 100 to 0.0001 hPa. Five days precede and 5 days follow the dates of the SSW peak in the stratosphere and mesosphere. The horizontal solid lines mark the altitude of ~90 km (0.003 hPa) and the stratospheric altitude ~25 km (10 hPa). The horizontal dotted lines mark the approximate altitude range of 82–98 km in which the majority of meteor trails are detected by the MR. This range is of the order of the MLS height resolution near 90 km altitude. The temperature profiles corresponding to the mesospheric cooling on 22 and 23 January are shown by dash lines. On 22–23 January, the MLS stratospheric temperature at 10 hPa is the largest while in the upper mesosphere at 0.01–0.005 hPa, the temperature experiences a minimum. A prominent thermal inversion layer of enhanced temperature that is at least 10 K greater than the background profile occurs near 90 km altitudes during the 2 day peak of SSW, while during other days the inversion is much less deep. Actually, at 90 km the temperature keeps the same value, 187 K, during 3 days including the day (21 January) preceding the SSW peak. However, while above 90 km the preceding day is cooler, the thermal inversion below 90 km is smaller.

The thermal inversion seen in Figure 6 enhances the temperatures inferred from MLS at 90 km (maximum of the meteor trials) as well as the temperatures averaged over the whole meteor layer at 82–98 km. The most prominent cooling is observed between ~82 and 88 km thus making these altitudes the most representative

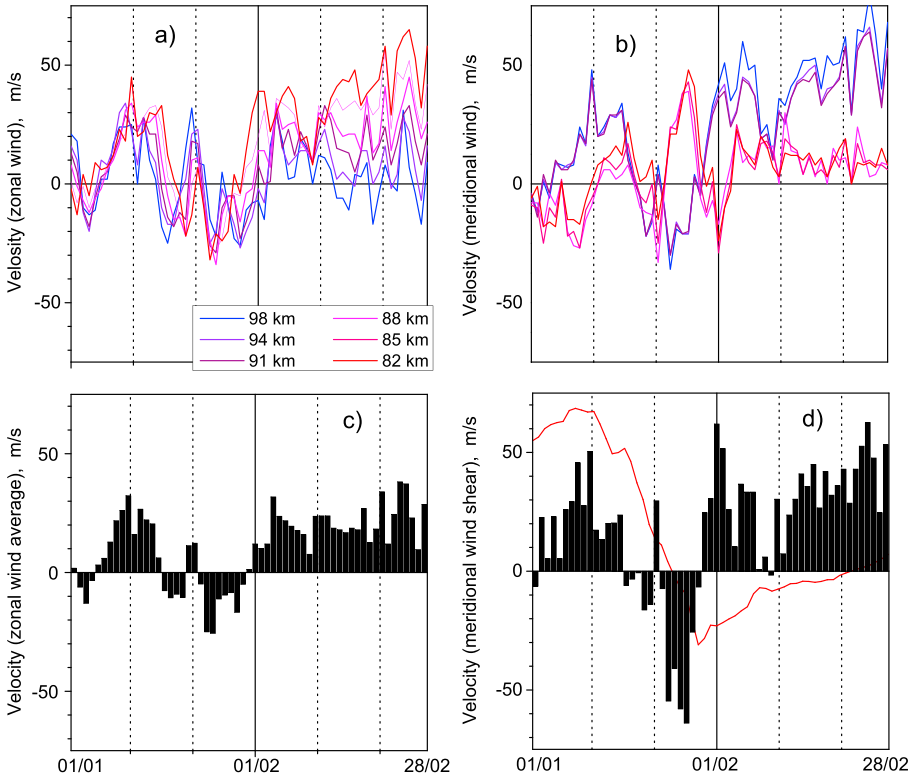


**Figure 7.** (a) Daily zonal and (b) meridional wind velocity at six height intervals from 82 to 98 km; (c) the altitudinally averaged zonal wind; (d) the difference between the upper (91–98 km) and lower (82–88 km) altitude meridional winds (the stratospheric zonal mean zonal wind from Figure 3b is also shown by red line) for a period of January–February 2009. Eastward and northward winds are positive.

for the temperature variation over the course of SSW. For this reason, the MLS temperatures averaged over 0.0046 and 0.001 hPa are taken for comparison with the values from the SGO MR (Figure 5).

### 5.3. Mesospheric Wind From SGO MR

In order to analyze the connection of mesospheric temperature fluctuations with circulation anomalies during the SSW under consideration, we explore the zonal and meridional winds observed with the SGO MR. To illustrate the altitudinal dependence of mesospheric winds, Figure 7 depicts the daily estimates of the prevailing zonal (Figure 7a) and meridional (Figure 7b) winds at each of the six height intervals from 82 to 98 km for a period from 1 January to 28 February 2009. The velocity of both, zonal and meridional, components varies between approximately −30 and +60 m/s (eastward and northward winds are positive). It is also seen that the mesospheric circulation is considerably intensified after the peak of the SSW.

The height distributions of the zonal and meridional components are qualitatively different. Zonal winds, especially before a SSW occurrence, exhibit similar variations at all altitudes. Except from the very beginning and the second half of January, when negative excursions (westward reversals) occur, the mesosphere is dominated by the eastward zonal wind. The most intense easterlies are developed in the course of SSW. After SSW, the zonal winds at all altitudes turn back to eastward with stronger wind flown below 90 km. The zonal wind evolution is summarized in Figure 7c where the daily values of the altitudinally averaged zonal wind are presented by vertical bars. Wind reversals from westerlies (up to ~30 m/s) to easterlies (up to ~25 m/s) are clearly seen on 2–4, 15–18, and 21–30 January.

The meridional winds are much less altitudinally uniform than the zonal one. Even visual inspection of Figure 7b reveals that the meridional winds split into two branches: below and above 90 km. The wind flow above 90 km is mostly northward with the only southward excursion in the second half of January, exactly at the same time the wind flow below 90 km turns north forming a meridional wind shear. The

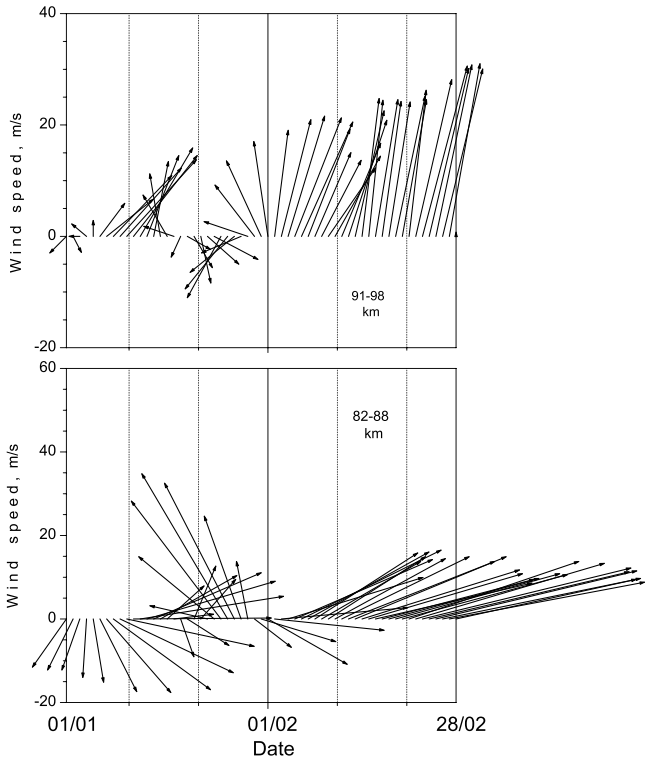


**Figure 8.** Daily mean of the wind velocity vectors averaged over the (top) 82–88 km and (bottom) 91–98 km height intervals for a period of January–February 2009.

magnitude of the shear is calculated as a difference between the wind flows within two height intervals above and below 90 km, i.e., the winds averaged over 82–88 km and those averaged over 91–98 km. The daily values of the meridional wind shear are displayed as vertical bars in Figure 7d. In 2009, large negative anomaly begins on 10 January and reaches maximum on 20 January. The meridional wind shear at the 90 km altitude is as large as 65 m/s/km.

Figure 8 shows the mesospheric wind evolution in more detail. In Figure 8 bottom (top), the daily mean of wind velocity vectors averaged over the 82–88 km (91–98 km) height intervals are presented. Both show considerable dynamic perturbations associated with the mesospheric cooling related to the SSW. Additional but small perturbation in the upper wind also occurred in the beginning of January. Before the onset of cooling in the mid-January, the velocity vector below (above) 90 km is directed to south-east (north-east). On 15 January, i.e., almost simultaneously with the beginning of stratospheric wind deceleration (see Figure 2b), the upper and lower wind vectors rotate clockwise and anticlockwise, respectively. When the mesospheric cooling reached its maximum, the upper winds turns southward while the lower wind is directed north-northwest. In late January, the mesosphere returns to the undisturbed conditions and the wind accelerates to unusually strong (up to 40 km/s) northward flow above 90 km which is likely driven by the seasonal pole-to-pole mesospheric circulation. The post-SSW wind flow below 90 km is eastward and equatorward reaching values up to 60 m/s.

## 6. Atmospheric Gravity Waves From the SGO Rapid-Run Ionosonde

The wind shear and other atmospheric turbulence affect the GW propagation and breaking. GWs play an important role in driving the mesospheric cooling during a SSW. At present, the SGO MR is not able to observe GW signatures and determine GW propagation direction in the MLT region. However, the simultaneous ionospheric measurements performed over Sodankyla make it possible to estimate GW presence in the ionosphere. Oscillations that originate in the lower atmosphere may propagate to the upper atmosphere and result in fluctuation and disturbance of the ionospheric electron density through dynamic coupling processes. To identify GW signatures in the ionosphere, the advantage of the SGO rapid-run ionospheric vertical ionosonde is used. In the data of vertical ionospheric soundings (ionograms), quasiperiodic oscillations of the *F* region virtual height with periods from a few minutes to several hours associated with traveling ionospheric disturbances (TIDs) are often observed. In most cases, TIDs are manifestations of atmospheric GWs at the altitude of 200–220 km. In the ionosphere, periods of GWs are larger than 10 min and the TIDs are detected in five bands of periods [*Kozlovsky et al.*, 2013]. The first band (periods from 5 to 10 min) corresponds to infrasonic waves and the GW cutoff band. The next four bands (10–15, 15–30, 30–60, and 60–120 min) span the small-scale (SS) to medium-scale (MS) and large-scale (LS) TIDs.

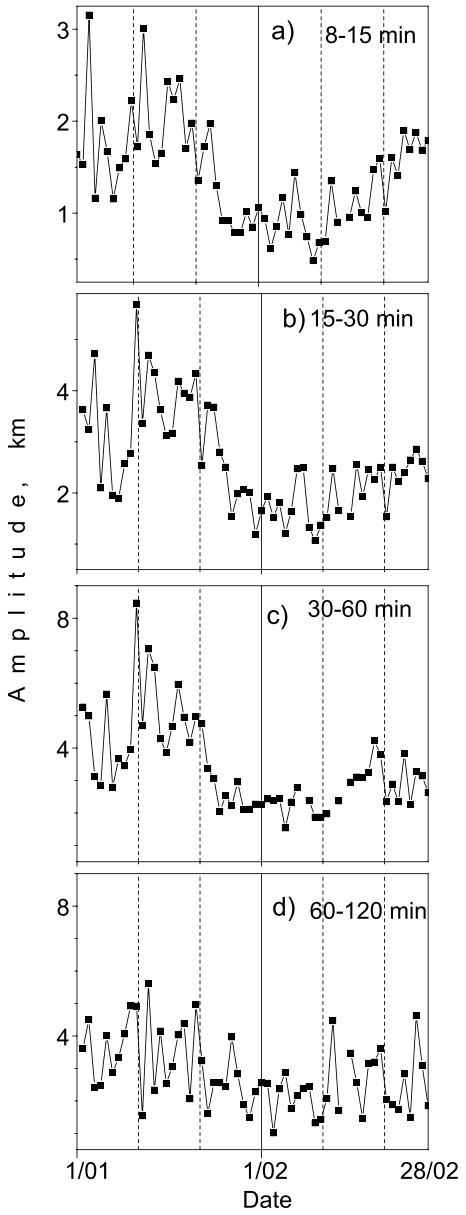


**Figure 9.** Mean daily amplitudes at 8–14 UT of GWs (TIDs) for four bands of periods (a) 10–15 min, (b) 15–30 min, (c) 30–60 min, and (d) 60–120 min from 1 January to 28 February 2009.

Figure 9 depicts the mean daily amplitudes at 8–14 UT (10–16 MLT) of GWs as manifested in TIDs measured by the SGO ionosonde from 1 January to 28 February 2009. Four bands from the shortest to the longest periods are shown. Examination of Figure 9 from top to bottom reveals that the SS (10–15 min) and MS (15–30 and 30–60 min) GWs abruptly decay after 20 January, i.e., just before the minimum of mesospheric temperature, while the LS (60–120 min) GWs are less affected. Thus, the relative contribution of the SS and MS considerably decreases, and only the LS waves reach the ionospheric height with less decay. The reduction begins almost simultaneously with the peak of the SSW and subsides until the end of February. The prolonged period of reduced GW coincides with the MLT cooling and with the rotation of the wind velocity vector from south-eastward to north-westward between 82 and 88 km. Since GWs often propagate against mean zonal winds, the westward mean flow in the MLT region filters out many of upward propagating westward GWs. Comparison of Figures 9 and 7 shows that after the end of January the reduced GW activity in the ionosphere can be readily explained by selective filtering of upward propagating westward GWs due to zonal winds, so that these waves do not reach the ionospheric $F_2$ layer. Small-scale vertical inhomogeneity and turbulence may also play a role in wave filtering and support its breaking.

## 7. Discussion

GW activity in the thermosphere is controlled by the selective filtering of GWs traveling upward from the lower atmosphere by changes in the stratospheric polar night jet and mesospheric winds. Since GWs tend to propagate against mean zonal winds, the eastward mean flow, for example, filters out many of upward propagating eastward GWs. Weakening of the stratospheric jet during a SSW permits eastward GW to penetrate into the MLT region. In the NH high latitudes between 20 and 60 km, the GW enhancements occur before the stratospheric jet reversal (from eastward to westward), and GWs become significantly weak after that [*Yamashita et al.*, 2010]. Recently, *de Wit et al.* [2014a] presented plausible observations of the westward GW forcing of the high-latitude mesopause region during the period of enhanced post-SSW eastward winds for a major SSW. However, the decay of GWs just after the wind reversal from eastward to westward and later after restoration of the eastward wind cannot be explained solely by filtering. It may be attributed to atmospheric turbulence. For example, coincident with the enhanced eastward winds after the SSW, *Hoffmann et al.* [2007] observed an increase of turbulent energy dissipation rates in the MLT. Also, the occurrence of the inversion layer (see Figure 6) manifests in increased turbulence in the MLT region: the topside of the inversion layer where the temperature decreases with increasing altitude may be convectively unstable. An additional consequence is the continued development of a shear region at 90 km altitude due to strong shear in the meridional

wind (see Figure 8). A critical layer with a Richardson number less than the threshold of 0.25 would be a potential reason of the turbulence. In addition to selective GWs filtering the turbulence may also play a role in the process of GWs occurrence reduction in the ionosphere. In particular, the turbulent viscosity is greater than molecular one. On the other hand, it is known that minimal permissible horizontal wavelength of GWs in the atmosphere is determined by viscosity and is proportional to the square root of it for the fixed wave frequency, whereas for the given viscosity the horizontal wavelength is proportional to $T^{3/2}$, where $T$ is a GW period [*Gossard and Hooke*, 1975]. Therefore, the result that GWs with periods 60–120 min are not affected by SSW can be explained by the fact that these waves have larger horizontal wavelengths.

The ionospheric response to SSW events was found at middle and equatorial latitudes [*Goncharenko and Zhang*, 2008; *Pancheva and Mukhtarov*, 2011], while the polar region is less investigated. Primarily, this is due to a lack of proper instrumentation to measure the GW amplitudes at thermospheric heights. From the theoretical side, *Yiğit and Medvedev* [2012] modeled the propagation of GWs of lower atmospheric origin to the thermosphere above the turbopause during a minor SSW. These authors demonstrated an enhancement and saturation of GW in the course of and after the end of SSW, respectively. This model prediction may partly explain the SGO MR observations of a decrease in GW amplitudes presented in Figure 9.

A major SSW occurred in the Arctic in January 2009. During SSW2009, the stratospheric zonally averaged temperature increases by ~50 K at 60°N, and the zonal wind reversal occurs at 10 hPa on 23 January. Different aspects of the stratosphere-mesosphere coupling during SSW2009 are described in a number of publications. It was shown that the SSW affects the winter middle atmosphere, causing significant variations in the MLT region [*Shepherd et al*., 2010; *Harada et al*., 2010; *Yue et al*., 2010; *Fuller-Rowell et al*., 2011; *Wang et al*., 2011; *Forbes and Zhang*, 2012; *Yamazaki et al*., 2012; *Liu et al*., 2014; *Iida et al*., 2014]. We found a clear signature of mesospheric cooling in concert with stratospheric warming. Radar and satellite observations over Sodankyla show that the stratospheric (~25 km) and mesospheric (~90 km) temperatures are clearly anticorrelated, which is in agreement with the common understanding of the wave-driven stratosphere-mesosphere coupling. The SGO MR and Aura EOS MLS show qualitatively very similar temperature variations, though the former is systematically ~30 K less than the latter. This difference may arise from different altitudes from which the radar and satellite temperatures are determined. The vertical distribution of meteor echoes is strongly peaked at heights near 90 km, while the analysis of the vertical temperature profiles from the Aura MLS shows that the temperature is the most variable at 0.01–0.002 hPa, i.e., between 82 and 90 km. At 90 km, an inversion layer is usually seen in the MLS profile. Also, there may be some calibration problem of the SGO MR. *Meek et al*. [2013]previously compared the Eureka, 80°N, MR temperatures with Aura MLS values and obtained generally good agreement between radar and satellite for winter temperatures but major difference (up to 25 K) in midsummer. The SGO MR seasonal values are not different from those from Eureka. However, to get temperatures from trail decay times, an on-site empirical estimate of the temperature gradient near 90 km is used [*Hocking*, 1999], and this parameter may affect the temperature. The SGO MR temperatures have not yet been systematically compared with the MLS data, and such analysis will be performed in the near future.

Recent studies found that the mesospheric cooling at high winter latitudes was observed several days before the onset of the SSW in the stratosphere [*Walterscheid et al*., 2000; *Dowdy et al*., 2004; *Mukhtarov et al*., 2007], while the model result of *Liu and Roble* [2002] for four consecutive years indicates little, if any, phase difference between the temperature anomalies in the mesosphere and stratosphere. In January 2009, the SGO MR local temperature minimum over Sodankyla was observed 1 day before the maximum at 10 hPa observed from space by the MLS. However, in January 2010, during medium SSW the mesospheric minimum occurred 4 days before the stratospheric maximum. It may be speculated that the lag depends on the SSW intensity and also on the increasing level of solar activity.

It has long been established that general circulation is changed dramatically in the stratosphere and mesosphere during SSW. While eastward zonal winds normally dominate the winter mesosphere, they turn westward in the course of a SSW that manifests stratosphere-mesosphere-upper atmosphere dynamical coupling. The timing and details of the wind reversal is not well established. *Dowdy et al*. [2004] showed that for the Southern Hemisphere major SSW in 2002, the zonal wind reversal in the mesosphere preceded that in the stratosphere by 1 week. Analysis of the Northern Hemisphere SSW in 2004 made by

[*Mukhtarov et al*., 2007] revealed that the mesosphere reversal of the zonal wind preceded the onset of the SSW at 10 hPa by almost 2 weeks. *Iida et al*. [2014] studied general circulation throughout the atmosphere associated with SSW2009 (Northern Hemisphere) and found that the reversal from westerly winds to easterly winds occurred 1 week earlier in the mesosphere in comparison with the stratopause level.

The SGO MR measurements provide the local view on the mesospheric wind reversal over Sodankyla. Routine data analysis yields hourly values of the zonal and meridional winds at six independent height intervals between 82 and 98 km. Analysis of the variation at each height interval reveals large-scale zonal and meridional anomalies linked to the major SSW under consideration. The SGO MR observes that the mesospheric wind begins to reverse almost simultaneously with the stratospheric wind deceleration. When the SSW is near its peak, a strong wind shear of 60–70 m/s/km occurs in the mesosphere so that the upper wind (above 90 km) turns clockwise from north-eastward to south-westward while the lower wind (below 90 km) turns anticlockwise from south-eastward to north-westward. It is notable that the meridional component is even more intense than the zonal one. Fast meridional transport of the opposite direction in the course of major SSW may be indicative for residual mean meridional circulation structures similar to those proposed by *Iida et al*. [2014] or warming in the lower mesosphere, while cooling occurs in the upper mesosphere [*Mukhtarov et al*., 2007]. After SSW, i.e., after a relaxation of temperatures toward radiative equilibrium, the SGO MR also observes some interesting features. In particular, the post-SSW wind behavior is characterized by considerably enhanced eastward and northward components below and above 90, respectively. The former is likely a signature of the polar jet strengthening in the upper stratosphere, while the latter may be considered as a part of interhemispheric meridional circulation developed at 30–90 km during solstice. The one-cell strato-mesospheric circulation is dominated by the upward flow in the summer hemisphere and the downward flow in the winter polar upper stratosphere/lower mesosphere.

The most prominent perturbations (especially in temperature) associated with a SSW is observed in the polar MLT region during a period of extremely low solar activity when the SSN was close to zero and the solar radio flux at 10.7 cm wavelength ($F_{10.7}$ index) was less than 70. Similar, though less prominent, signatures are observed during the medium SSW in 2010. In 2013, when the solar activity level is high, the zonal wind reversal is marginal, the meridional wind shear is short lived, and no mesospheric cooling is detected by the SGO MR. We speculate that a weak response of the auroral mesosphere to the major SSW in 2013 winter is caused the high solar activity. However, the 6 year period of continuous observations over Sodankyla spans one solar minimum and one solar maximum only. Further observations are needed to make a decisive conclusion on the role of solar activity in the middle-upper atmosphere coupling during a SSW.

## 8. Conclusion

Thermal structures of the warm winter (~175 K) and cold summer (~100 K) high-latitude mesopause temperatures have been observed by the SGO MR for over 6 years from 2008 onward. North-eastward winds normally dominate the winter mesosphere. These prevailing winds turn to the opposite direction when strong thermal and dynamical perturbations occur in relation with SSWs. Under conditions of low solar activity, pronounced sudden mesospheric coolings linked to the major SSW2009 and medium SSW in 2010 are observed while no thermal mesospheric signature of the major SSW in 2013, that occurred during the solar maximum, is observed. Considerable strengthening of the northward winds up to 90 km and eastward winds below 90 km is characteristics of the post-SSW period independent of solar activity level.

Mesosphere-ionosphere anomalies observed simultaneously by the SGO MR, the Aura EOS MLS, and the rapid-run ionosonde over Sodankyla during a period of the major SSW2009 include the following features.

1. Mesospheric cooling is almost of the same value as the stratospheric warming (~50 K) but the former decay faster than the latter. The mesospheric minimum occurs 1 day ahead of the stratospheric maximum. Deepening of the thermal inversion layer is observed near 90 km altitude during the peak of SSW/mesospheric cooling.
2. In the course of a SSW, a strong wind shear of 60–70 m/s/km occurs so that the wind turns clockwise (anticlockwise) from north-eastward (south-eastward) to south-westward (north-westward) up (below) to 90 km.
3. Just after the mesospheric temperature reaches its minimum, the GWs occurrence in the ionosphere with periods of 10–60 min decay abruptly while the GWs with longer periods are not affected. The effect of

such weakening of the mesosphere-ionosphere coupling may be explained by selective filtering and/or increased turbulence near the mesopause.

**Acknowledgments**
The authors appreciate the NASA for access to the Aura MLS data from http://disc.sci.gsfc.nasa.gov/Aura/data-holdings/MLS/index.shtml and the solar indices from CDAWeb (http://omniweb.gsfc.nasa.gov/). MERRA results are available through http://disc.sci.gsfc.nasa.gov/daac-bin/DataHoldings.pl. Data of the meteor radar and ionosonde are available from SGO (http://www.sgo.fi/). R.L. and S.S. acknowledge support from the Academy of Finland grant 276824 and Russian MoES grant 14.607.21.0058. M. L. acknowledges support from NERC via NERC grant NE/K011766/1.

Alan Rodger thanks Indrani Roy and one anonymous reviewer for their assistance in evaluating this paper.

## References

Andrews, D. G., J. R. Holton, and C. B. Leovy (1987), *Middle Atmospheric Dynamics*, 489 pp., Elsevier, New York.
Cho, Y.-M., G. G. Shepherd, Y.-I. Won, S. Sargoytchev, S. Brown, and B. Solheim (2004), MLT cooling during stratospheric warming events, *Geophys. Res. Lett.*, *31*, L10104, doi:10.1029/2004GL019552.
De Wit, R. J., R. E. Hibbins, P. J. Espy, Y. J. Orsolini, V. Limpasuvan, and D. E. Kinnison (2014a), Observations of gravity wave forcing of the mesopause region during the January 2013 major sudden stratospheric warming, *Geophys. Res. Lett.*, *41*, 4745–4752, doi:10.1002/2014GL060501.
De Wit R. J., R. E. Hibbins, and P. J. Espy (2014b), The seasonal cycle of gravity wave momentum flux and forcing in the high latitude Northern Hemisphere mesopause region, *J. Atmos. Sol. Terr. Phys.*, doi:10.1016/j.jastp.2014.10.002
Dowdy, A. J., R. A. Vincent, D. J. Murphy, M. Tsutsumi, D. M. Riggin, and M. J. Jarvis (2004), The large-scale dynamics of the mesosphere-lower thermosphere during the Southern Hemisphere stratospheric warming of 2002, *Geophys. Res. Lett.*, *31*, L14102, doi:10.1029/2004GL020282.
Dyrland, M., E. Hall, C. M. Mulligan, F. J. Tsutsumi, and M. F. Sigernes (2010), Improved estimates for neutral air temperatures at 90 km and 78 N using satellite and meteor radar data, *Radio Sci.*, *45*, RS4006, doi:10.1029/2009RS004344.
Forbes, J. M., and X. Zhang (2012), Lunar tide amplification during the January 2009 stratosphere warming event: Observations and theory, *J. Geophys. Res.*, *117*, A12312, doi:10.1029/2012JA017963.
Fuller-Rowell, T., H. Wang, R. Akmaev, F. Wu, T.-W. Fang, M. Iredell, and A. Richmond (2011), Forecasting the dynamic and electrodynamic response to the January 2009 sudden stratospheric warming, *Geophys. Res. Lett.*, *38*, L13102, doi:10.1029/2011GL047732.
Goncharenko, L., and S.-R. Zhang (2008), Ionospheric signatures of sudden stratospheric warming: Ion temperature at middle latitude, *Geophys. Res. Lett.*, *35*, L21103, doi:10.1029/2008GL035684.
Gossard, E., and W. Hooke (1975), *Waves in the Atmosphere*, 456 pp., Elsevier, New York.
Harada, Y., A. Goto, H. Hasegawa, N. Fujikawa, H. Naoe, and T. Hirooka (2010), A major stratospheric sudden warming event in January 2009, *J. Atmos. Sci.*, *67*, 2052–2069, doi:10.1175/2009JAS3320.1.
Hocking, W. K. (1999), Temperatures using radar-meteor decay times, *Geophys. Res. Lett.*, *26*(21), 3297–3300, doi:10.1029/1999GL003618.
Hocking, W. K., B. Fuller, and B. Vandepeer (2001), Real-time determination of meteor-related parameters utilizing modern digital technology, *J. Atmos. Sol. Terr. Phys.*, *63*, 155–169.
Hoffmann, P., W. Singer, and D. Keuer (2002), Variability of the mesospheric wind field at middle and Arctic latitude in winter and its relation to stratospheric circulation disturbances, *J. Atmos. Sol. Terr. Phys.*, *64*, 1229–1240.
Hoffmann, P., W. Singer, D. Keuer, W. K. Hocking, M. Kunzec, and Y. Murayama (2007), Latitudinal and longitudinal variability of mesospheric winds and temperatures during stratospheric warming events, *J. Atmos. Sol. Terr. Phys.*, *69*(17–18), 2355–2366, doi:10.1016/j.jastp.2007.06.010.
Iida, C., T. Hirooka, and N. Eguchi (2014), Circulation changes in the stratosphere and mesosphere during the stratospheric sudden warming event in January 2009, *J. Geophys. Res. Atmos.*, *119*, 7104–7115, doi:10.1002/2013JD021252.
Kim, J.-H., Y. H. Kim, G. Jee, and C. Lee (2012), Mesospheric temperature estimation from meteor decay times of weak and strong meteor trails, *J. Atmos. Sol. Terr. Phys.*, *89*, 18–26.
Kozlovsky, A., T. Turunen, and T. Ulich (2013), Rapid-run ionosonde observations of traveling ionospheric disturbances in the auroral ionosphere, *J. Geophys. Res. Atmos.*, *118*, 5265–5276, doi:10.1002/jgra.50474.
Kozlovsky, A., S. Shalimov, R. Lukianova, and M. Lester (2014), Ionospheric effects of the missile destruction on 9 December 2009, *J. Geophys. Res. Space Physics*, *119*, 3873–3882, doi:10.1002/2013JA019531.
Labitzke, K. (1972), Temperature changes in the mesosphere and stratosphere connected with circulation changes in winter, *J. Atmos. Sci.*, *29*, 756–766.
Labitzke, K., and B. Naujokat (2000), The lower arctic stratosphere in winter since 1952, *SPARC Newslett.*, *15*, 11–14.
Labitzke, K., and M. Kunze (2009), On the remarkable Arctic winter in 2008/2009, *J. Geophys. Res.*, *114*, D00I02, doi:10.1029/2009JD012273.
Liu, H., Y. Miyoshi, S. Miyahara, H. Jin, H. Fujiwara, and H. Shinagawa (2014), Thermal and dynamical changes of the zonal mean state of the thermosphere during the 2009 SSW: GAIA simulations, *J. Geophys. Res. Space Physics*, *119*, 6784–6791, doi:10.1002/2014JA020222.
Liu, H.-L., and R. G. Roble (2002), A study of a self-generated stratospheric sudden warming and its mesospheric-lower thermospheric impacts using the coupled TIMEGCM/CCM3, *J. Geophys. Res.*, *107*, 4695–4712, doi:10.1029/2001JD001533.
Livesey, N. J., et al. (2013), EOS MLS version 3.3 level 2 data quality and description document, Rep. JPLD-33509, Version 3.3x-1.0, Jet Propul. Lab., Calif. Inst. of Technol., Pasadena. [Available at http://mls.jpl.nasa.gov/data/v3-3_data_quality_document.pdf.]
Lysenko, I. A., Y. I. Portnyagin, K. M. Greisigerm, and K. Sprenger (1975), Some peculiarities of the atmospheric circulation at the altitude of 90–100 km over Europe in winter 1972–73, *J. Meteorol.*, *25*, 213–217.
Manson, A. H., et al. (2011), Characteristics of Arctic winds at CANDAC-PEARL (80°N, 86°W) and Svalbard (78°N, 16°E) for 2006–2009: Radar observations and comparisons with the model CMAMDAS, *Ann. Geophys.*, *29*, 1927–1938, doi:10.5194/angeo-29-1927-2011.
Matsuno, T. (1971), A dynamical model of the stratospheric sudden warming, *J. Atmos. Sci.*, *28*, 1479–1494.
Meek, C. E., A. H. Manson, W. K. Hocking, and J. R. Drummond (2013), Eureka, 80°N, SKiYMET meteor radar temperatures compared with Aura MLS values, *Ann. Geophys.*, *31*, 1267–1277, doi:10.5194/angeo-31-1267-2013.
Meriwether, J. W., and A. J. Gerrard (2004), Mesosphere inversion layers and stratosphere temperature enhancements, *Rev. Geophys.*, *42*, RG3003, doi:10.1029/2003RG000133.
Mukhtarov, P., et. al. (2007), Large-scale thermodynamics of the stratosphere and mesosphere during the major stratospheric warming in 2003/2004, *J. Atmos. Sol. Terr. Phys.*, *69*(17–18), 2338–2354.
Pancheva, D., and P. Mukhtarov (2011), Stratospheric warmings: The atmosphere–ionosphere coupling paradigm, *J. Atmos. Sol. Terr. Phys.*, *73*, 1697–1702.
Rienecker, M. M., et al. (2011), MERRA: NASA's Modern-Era Retrospective Analysis for Research and Applications, *J. Clim.*, *24*, 3624–3648, doi:10.1175/JCLI-D-11-00015.1.
Russell, C. T., J. G. Luhmann, and L. K. Jian (2010), How unprecedented a solar minimum?, *Rev. Geophys.*, *48*, RG2004, doi:10.1029/2009RG000316.
Shepherd, M. G., Y.-M. Cho, G. G. Shepherd, W. Ward, and J. R. Drummond (2010), Mesospheric temperature and atomic oxygen response during the January 2009 major stratospheric warming, *J. Geophys. Res.*, *115*, A07318, doi:10.1029/2009JA015172.
Siskind, D. E., L. Coy, and P. Espy (2005), Observations of stratospheric warmings and mesospheric coolings by the TIMED SABER instrument, *Geophys. Res. Lett.*, *32*, L09804, doi:10.1029/2005GL022399.

Walterscheid, R. L., G. G. Sivjee, and R. G. Roble (2000), Mesospheric and lower thermospheric manifestation of a stratospheric warming event over Eureka, Canada (80°N), *Geophys. Res. Lett.*, *27*, 2897–2900, doi:10.1029/2000GL003768.

Wang, H., T. J. Fuller-Rowell, R. A. Akmaev, M. Hu, D. T. Kleist, and M. D. Iredell (2011), First simulations with a whole atmosphere data assimilation and forecast system: The January 2009 major sudden stratospheric warming, *J. Geophys. Res.*, *116*, A12321, doi:10.1029/2011JA017081.

Waters, J. W., et al. (2006), The Earth Observing System Microwave Limb Sounder (EOS MLS) on the Aura satellite, *IEEE T. Geosci. Rem.*, *44*(5), 1075–1092.

World Meteorological Organization Commission for Atmospheric Sciences (1978), WMO Commission for Atmospheric Sciences Abridged Final Report of the Seventh Session, Manila, 27 February- 10 March 1978. WMO No. 509. (p. 36, item 9.4.4).

Yamashita, C., H.-L. Liu, and X. Chu (2010), Gravity wave variations during the 2009 stratospheric sudden warming as revealed by ECMWF T799 and observations, *Geophys. Res. Lett.*, *37*, L22806, doi:10.1029/2010GL045437.

Yamazaki, Y., A. D. Richmond, H. Liu, K. Yumoto, and Y. Tanaka (2012), Sq current system during stratospheric sudden warming events in 2006 and 2009, *J. Geophys. Res.*, *117*, A12313, doi:10.1029/2012JA018116.

Yiğit, E., and A. S. Medvedev (2012), Gravity waves in the thermosphere during a sudden stratospheric warming, *Geophys. Res. Lett.*, *39*, L21101, doi:10.1029/2012GL053812.

Yue, X., et. al. (2010), Global ionospheric response observed by COSMIC satellites during the January 2009 stratospheric sudden warming event, *J. Geophys. Res.*, *115*, A00G09, doi:10.1029/2010JA015466.